Applied Catalysis B: Environmental 158–159 (2014) 382–390

Contents lists available at ScienceDirect

Applied Catalysis B: Environmental

journal homepage: www.elsevier.com/locate/apcatb

Coupled systems for selective oxidation of aromatic alcohols to aldehydes and reduction of nitrobenzene into aniline using CdS/g-C_3N_4 photocatalyst under visible light irradiation

Xia Dai[a,b], Mengli Xie[b], Sugang Meng[b], Xianliang Fu[b], Shifu Chen[a,b,*]

[a] Department of Chemistry, Anhui Science and Technology University, Anhui Fengyang 233100, People's Republic of China
[b] Department of Chemistry, Huaibei Normal University, Anhui Huaibei 235000, People's Republic of China

ARTICLE INFO

Article history:
Received 5 February 2014
Received in revised form 15 April 2014
Accepted 19 April 2014
Available online 26 April 2014

Keywords:
CdS/g-C_3N_4
Selective oxidation
Reduction
Coupled system
Photocatalysis

ABSTRACT

A coupled system of selective oxidation of aromatic alcohols to aromatic aldehydes and reduction of nitrobenzene into aniline was realized using CdS/g-C_3N_4 composite as a photocatalyst under visible light illumination. The CdS/g-C_3N_4 composite photocatalyst was prepared by hydrothermal method. The photocatalyst was characterized by x-ray powder diffraction (XRD), UV–vis diffuse reflection spectroscopy (DRS), scanning electron microscopy (SEM), transmission electron microscopy (TEM), and Brunauer–Emmett–Teller (BET) specific surface area. Compared with single g-C_3N_4 and CdS, the CdS/g-C_3N_4 photocatalyst exhibits enhanced photocatalytic activity and excellent photostability under visible light illumination. It demonstrates that the selective oxidation of aromatic alcohol into aromatic aldehyde is achieved by direct holes oxidation, and the reduction of nitrobenzene into aniline is reached by direct electrons reduction. The optimum percentage of CdS is 10 wt.%. Under illumination for 4 h, the conversion of benzyl alcohol and the yield of benzaldehyde are about 48.0% and 44.6%, and the conversion of nitrobenzene and the yield of aniline are about 49.2% and 26.0%, respectively. The synergic effect of g-C_3N_4 and CdS, which can effectively separate and transfer photoexcited carriers, was proposed to be responsible for the enhancement of the photocatalytic activity. This study has a guiding significance for the design of a coupled system which realizes selective oxidation and reduction of organics.

1. Introduction

The photocatalysis technology has attracted much attention since 1972 when Fujishima and Honda found that single TiO_2 electrode can split water into hydrogen and oxygen [1–3]. At present, the research work for the photocatalysis mainly focuses on the degradation of pollutants in air and water, producing hydrogen from water splitting and selective transformation of organics [4–10]. It is worth noting that the selective oxidation and reduction of organics for the synthesis of organic compounds using photocatalytic method have attracted attention in recent years [11–14].

Aromatic aldehydes and their derivatives are important fine chemical intermediates. Traditional oxidants used in the oxidation process of aromatic alcohol usually have toxicity or corrosivity, such as $KMnO_4$, CrO_3, ClO^- and Cl_2. It has been reported that semiconductor photocatalysts can be applied in the selective oxidation of $-CH_2OH$ to $-CHO$ instead of CO_2 and H_2O [11,12]. For example, the modified TiO_2, M/TiO_2 (M = Au, Pd, Pt) and Pd@CeO_2, etc. have been proved to be excellent photocatalysts for the selective oxidation of aromatic alcohols to corresponding aromatic aldehydes [15–17]. Furthermore, Zhao and coworkers have researched the aerobic oxidation of alcohols to corresponding aldehydes using a special coupled system consisting of dye-sensitized TiO_2 and TEMPO (2,2,6,6-tetramethypiperdinyloxyl) under visible light illumination [18]. However, the conversion of benzyl alcohol and the yield of benzaldehyde are fairly low in the reported results. The reason may be that TiO_2 has strong oxidation ability due to its positive valence band (VB) of 2.7 eV and wide energy gap of 3.2 eV (vs. NHE pH 7). Furthermore, it has also been reported that mpg-C_3N_4 polymer is an excellent photocatalyst for the selective oxidation of alcohols and hydrocarbons [19,20]. At the same time, many papers have also reported a series of CdS nanomaterials for the selective oxidation of alcohols, alkenes and toluene in a liquid phase under ambient conditions [21–23]. Therefore, improving the performance of photocatalysts has always been a research hot spot. Recently, many attempts have been explored to enhance the activities of g-C_3N_4 and CdS photocatalysts, such as the synthesis of quantum

* Corresponding author at: Corresponding author. Tel.: +86 561 3806611; fax: +86 561 3090518.
E-mail address: chshifu@chnu.edu.cn (S. Chen).

http://dx.doi.org/10.1016/j.apcatb.2014.04.035
0926-3373/

dots [24,25] and the combination with other components, including noble metals [26–30], semiconductors [31–36], and carbon materials, etc. [37–40].

Aniline is one of the most important chemicals and intermediates in the production of pharmaceuticals, dyes, pigments and pesticides [41,42]. In general, catalytic hydrogenation method has been commonly used to reduce nitrobenzene (NB) to aniline [41–43]. But, the reaction needs to be performed at high temperature, high pressure of H_2, and a long time in order to reach a satisfied selectivity of aniline [43,44]. In recent years, photocatalytic reduction of nitrobenzene into aniline using photocatalytic technology has been reported in some literatures [45–47]. However, the reduction process of nitrobenzene needs to use organic compounds such as methanol ethanol as a hole scavenger. Furthermore, the reactant conversion and product selectivity are also unsatisfactory [45,47]. Theoretically, when the conduction band (CB) potential of a photocatalyst is lower than −0.486 V, nitrobenzene can be photocatalytically reduced into aniline (E^{Θ} ($C_6H_5NO_2/C_6H_5NH_2$) = −0.486 V, vs. NHE) [45].

Based on the reported results, designing new narrow band gap semiconductor photocatalysts that have high CB negative values and appropriate VB position may be an effective method for selective oxidation of aromatic alcohols to aldehydes and reduction of nitrobenzene into aniline in a reaction system. It is known that the VB potentials of g-C_3N_4 and CdS are about 1.57 and 1.88 eV, and CB potentials of g-C_3N_4 and CdS are −1.13 and −0.5 eV, respectively [48,49]. According to the reported results, it is proposed that g-C_3N_4 and CdS have ability for the selective oxidation of alcohols to aldehydes and the reduction of nitrobenzene to aniline. It has been reported that designing composite photocatalysts were considered as the most effective way to overcome the defects of single-phase photocatalysts because the photoexcited carriers are transferred into VB and CB of opposite semiconductor, respectively [50–52]. Hence, when g-C_3N_4 and CdS are combined, a composite photocatalyst CdS/g-C_3N_4 may be formed, and the photocatalytic activity may be improved greatly. However, to the best of our knowledge, there is no report on the investigation of the related issues.

In the paper, the CdS/g-C_3N_4 composite photocatalyst was prepared by hydrothermal method. A coupled system for the selective oxidation of aromatic alcohols to aldehydes and the reduction of nitrobenzene into aniline was realized using CdS/g-C_3N_4 photocatalyst under visible light illumination with N_2 purge condition. The obtained CdS/g-C_3N_4 composites show significantly improved photocatalytic performance in contrast to pure g-C_3N_4 and CdS. Meanwhile, the CdS/g-C_3N_4 photocatalyst exhibits high stability. It is proposed that the selective oxidation of aromatic alcohol into aromatic aldehyde is realized by direct holes oxidation, and the reduction of nitrobenzene into aniline is achieved by direct electrons reduction. The work strongly substantiates the feasibility for the selective oxidation and reduction of organics in a coupled system. The CdS/g-C_3N_4 composite photocatalyst is a promising and efficient photocatalyst for the selective oxidation of aromatic alcohols to aldehydes and the reduction of nitrobenzene into aniline.

2. Experimental

2.1. Materials

All reagents are of analytical purity and were used without further purification. Melamine ($C_3H_3N_6$) powder, cadmium acetate ($Cd(CH_3COO)_2{\cdot}2H_2O$), thioacetamide (TAA), ethanol (C_2H_5OH) and other reagents used in the experiments were obtained from Sinopharm Chemical Reagent Co., Ltd. Deionized water was used throughout this study.

2.2. Preparation of photocatalysts

The g-C_3N_4 powder was synthesized via calcination method in air atmosphere. A certain amount of melamine was put into an alumina crucible which was firstly heated at 500 °C for 2 h and further heated at 520 °C for 2 h with a temperature rise rate of 10 °C/min. Then the sample was cooled naturally to room temperature after the reaction. The synthesis of CdS/g-C_3N_4 composite was carried out as follows: after adding 2 mmol of $Cd(CH_3COO)_2{\cdot}2H_2O$ and 4 mmol TAA into 50 ml deionized water and stirring for 30 min, the solution A was obtained. A measured amount of g-C_3N_4 sample was added to the solution A, and was stirred for 1 h. The obtained suspension was transferred into a 100 mL teflon-lined stainless steel autoclave, and then was heated to 180 °C and kept at this temperature for 24 h. With the above method, a series of CdS/g-C_3N_4 composites with various amounts of CdS were prepared. After being cooled naturally to room temperature, the product was collected and washed using water and ethanol for 3 times, repeatedly. The pure CdS photocatalyst was obtained by the same conditions without adding g-C_3N_4 powder.

2.3. Characterization

XRD measurements were carried out at room temperature on a BRUKER D8 ADVANCE X-ray powder diffractometer with Cu Kα radiation (k = 1.5406 Å) and a scanning speed of 3°/min. The accelerating voltage and emission current were 40 kV and 30 mA, respectively. UV–vis diffuse reflectance spectra (DRS) were carried out using a UV-3600 (SHIMA-DZU, Japan) UV–vis–NIR spectrophotometer equipped with an integrating sphere attachment. $BaSO_4$ was used as a reflectance standard. The microcrystalline structure and surface characteristics of photocatalysts were measured using a JEOL JSM-6610LV scanning electron microscope with 30 kV scanning voltages. Transmission electron microscopy (TEM) and high-resolution transmission electron microscopy (HR-TEM) images were performed with a JEM-2100 electron microscope, using an accelerating voltage of 200 kV. The nitrogen adsorption and desorption isotherms at 77 K were measured using a Micrometrics ASAP 2020 system after the samples were degassed in vacuum at 120 °C for 8 h. The Brunauer–Emmett–Teller (BET) specific surface area was determined by a multipoint BET method using the adsorption data in the relative pressure (P/P_0) range of 0.05–0.25.

2.4. Evaluation of photocatalytic activity

The photocatalytic activities of photocatalysts for the selective oxidation of aromatic alcohols to corresponding aromatic aldehydes and the reduction of nitrobenzene into aniline were performed in a self-designed photochemical reactor equipped with a pressure gage which is convenient for monitoring the pressure in the autoclave. The reaction apparatus is shown in Fig. 1. The initial concentrations of aromatic alcohol and NB were 2.55×10^{-2} mol/L and 8.5×10^{-3} mol/L, respectively. 15 ml reaction solution (benzotrifluoride as solvent) containing reactants and 0.1 g photocatalyst were put into a 100 ml reactor of Teflon-lined stainless steel autoclave. The illumination window on the top of the reactor is made of high strength quartz glass. Before illumination, nitrogen was passed through the solution for 0.5 h to remove the dissolved oxygen, and maintained in the reactor at a pressure of 0.5 MPa. A 300 W Xe arc lamp (PLS-SXE 300, Beijing Perfect light Co., Ltd.) with a UV–CUT filter to cut off light of wavelength $\lambda < 420$ nm was used as the irradiation source. Owing to continuous cooling with the refrigeration circulating water, the temperature of the reaction solution was maintained at approximately 60 °C. The mixture was stirred in the dark for 1 h to ensure the adsorption–desorption equilibrium between the photocatalyst and reactant. After illumination for

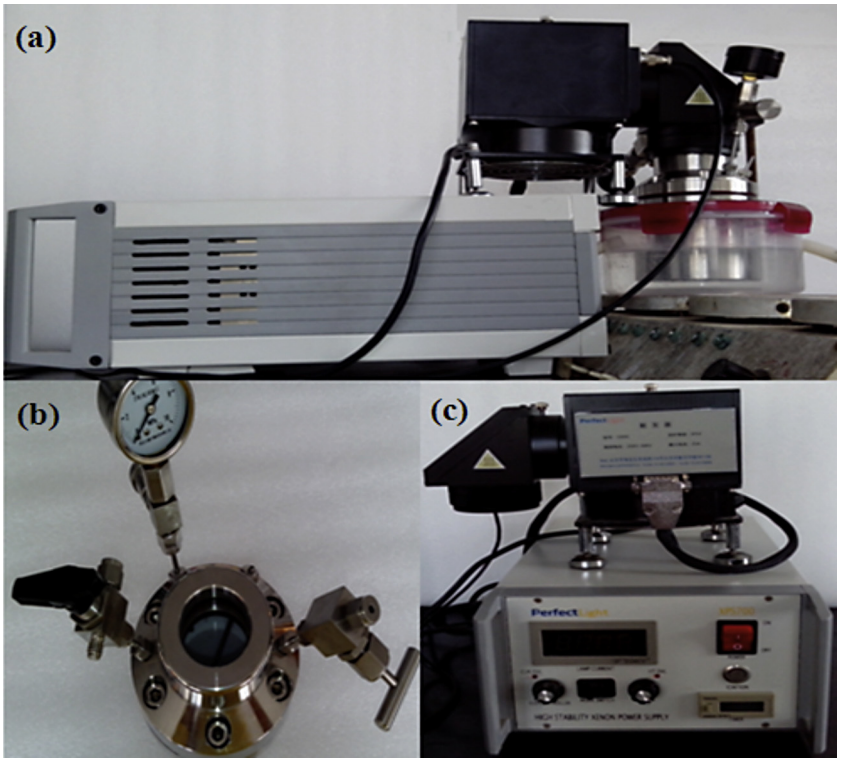

Fig. 1. The apparatus of photocatalytic reaction. (a) apparatus; (b) reactor; (c) light source

4 h, the reaction solution was collected from the reactor and centrifuged to remove the catalyst completely at 4000 rmp for 20 min, and finally filtered through a 0.2-μm millipore filter to remove any residual particles.

2.5. Analysis of main products

The main product of selective oxidation of aromatic alcohols is aromatic aldehydes, and the reduction product of NB is aniline. The solution was analyzed by Gas-Chromatography (Fuli 9790, China) with FID detector using a SE-30 0.53 mm × 30 m capillary column (GC conditions: chromatographic column: AC20; carrier gas: N_2; flow rate: 30 ml/min; sample injection volume: 0.2 μl). Conversion of alcohol, yield of aldehyde, and selectivity for aldehyde were defined as follows [17]:

$$\text{Conversion}(\%) = [(C_0 - \text{Calcohol})/C_0] \times 100 \quad (1)$$

$$\text{Yield}(\%) = \text{Caldehyde}/C_0 \times 100 \quad (2)$$

$$\text{Selectivity}(\%) = [\text{Caldehyd}/(C_0 - \text{Calcohol})] \times 100 \quad (3)$$

Where C_0 is the whole amount of alcohols in the solution before illumination; $C_{alcohol}$ is the amount of alcohols in the solution after illumination for 4 h; $C_{aldehyde}$ is the amount of aldehyde in the solution after illumination for 4 h.

The reduction of nitrobenzene was calculated as follows:

$$\text{Conversion}(\%) = [(C_0 - C_{NB})/C_0] \times 100 \quad (4)$$

$$\text{Yield}(\%) = C_{aniline}/C_0 \times 100 \quad (5)$$

$$\text{Selectivity}(\%) = [\text{Caniline}/(C_0 - C_{NB})] \times 100 \quad (6)$$

Where C_0 is the whole amount of NB in the solution before illumination; C_{NB} is the amount of NB in the solution after illumination for 4 h; $C_{aniline}$ is the amount of aniline in the solution after illumination for 4 h.

3. Results and discussion

3.1. Characterization of photocatalysts

3.1.1. XRD analysis

In order to determine the crystal phase composition and the crystallite size of the photocatalyst, XRD study was carried out. Fig. 2 shows the XRD patterns of CdS/g-C_3N_4 composites with different amounts of CdS. The XRD patterns of pure CdS and g-C_3N_4 are also given for comparison. It is clear that the pure g-C_3N_4 sample has two distinct peaks at 13.1°and 27.4°, which can be indexed as (1 0 0) and (0 0 2) diffraction planes for graphitic materials [53,54]. The former with a much weaker intensity, which corresponds to a distance d = 0.676 nm, is related to an in-plane structural packing motif; the latter which corresponds to the interlayer distance of 0.325 nm, is attributed to the long-range interplanar stacking of aromatic systems. The two peak intensities decrease quickly with

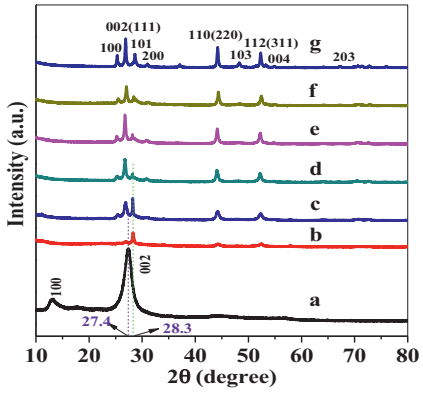

Fig. 2. XRD patterns of the different samples.
(a) g-C_3N_4, (b) CdS(1.0 wt.%)/g-C_3N_4, (c) CdS(5.0 wt.%)/g-C_3N_4, (d) CdS(10.0 wt.%)/g-C_3N_4, (e) CdS (15.0 wt.%)/g-C_3N_4, (f) CdS(20.0 wt.%)/g-C_3N_4, (g) CdS

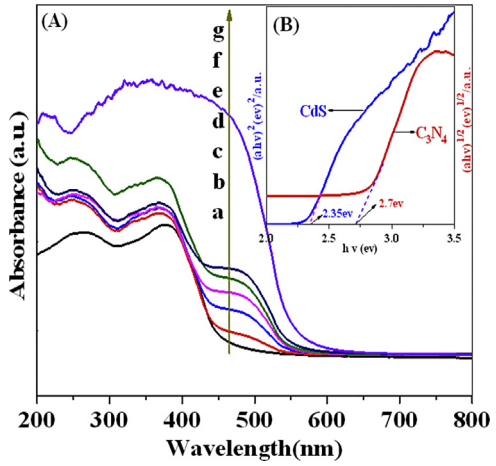

Fig. 3. UV–vis diffuse reflectance spectra of the different samples. (a) g-C_3N_4, (b) CdS (1.0 wt.%)/g-C_3N_4, (c) CdS (5.0 wt.%)/g-C_3N_4, (d) CdS (10.0 wt.%)/g-C_3N_4, (e) CdS (15.0 wt.%)/g-C_3N_4, (f) CdS (20.0 wt.%)/g-C_3N_4, (g) CdS

the increase of introduced CdS. Furthermore, the (0 0 2) diffraction peak shifts to high angle from 27.4° to 28.3°, and this may be attributed to the strong interreaction between g-C_3N_4 and CdS resulting in the increase of the interlayer spacing of g-C_3N_4. When the amount of CdS is higher than 5%, there is no obvious diffraction peak of g-C_3N_4, suggesting that CdS nanoparticles have been successfully deposited onto the surface of C_3N_4. And with the increase in the amount of CdS, the diffraction peaks of CdS gradually strengthen. On the basis of Scherrer formula, the calculated average crystallite size of CdS particle is about 13.5 nm. Furthermore, the as-prepared CdS is a mixture of hexagonal and cubic phases by comparing with the JCPDS card files no. 41-1049 and 10-0454. The (1 0 0), (0 0 2), (1 0 1) diffraction peaks belong to hexagonal phase and the (2 0 0) diffraction peak is attributed to cubic phase. Other diffraction peaks are also attributed to the two phases. The CdS/g-C_3N_4 samples exhibit diffraction peaks corresponding to both g-C_3N_4 and CdS, and no other impure peaks can be observed, suggesting that the samples are composed of g-C_3N_4 and CdS.

3.1.2. UV–vis analysis

The optical property of CdS/g-C_3N_4 was determined by UV–vis diffuse reflectance spectroscopy. Fig. 3 depicts UV–vis absorption spectra of the prepared CdS/g-C_3N_4, pure g-C_3N_4 and CdS. The pristine g-C_3N_4 shows its fundamental absorption edge rising at 460 nm, which can be assigned to its intrinsic band gap of 2.7 eV. The pure CdS sample has an absorption edge at about 528 nm, which can be attributed to the CdS band gap of 2.35 eV. However, the spectra of CdS/g-C_3N_4 samples show two absorption edges, suggesting that the samples contain two semiconductors of CdS and g-C_3N_4. The absorption edges at about 460 nm and 528 nm are ascribed to g-C_3N_4 and CdS, respectively. Compared with the pure C_3N_4, it is clear that the absorption wavelength range of CdS/g-C_3N_4 sample appears red shift. It may be favorable for the use of the visible light and the enhancement of the photocatalytic activity of the samples. For a crystalline semiconductor, the optical absorption near the band edge follows the formula [55]:

$$ahv = A(hv - Eg)^{n/2} \quad (7)$$

where *a*, *v*, *A*, and *Eg* are the absorption coefficient, light frequency, proportionality coefficient, and band gap energy, respectively. *n* keys the properties of the transition in a semiconductor ($n = 1$ for direct transition, and $n = 4$ for indirect transition). The values of n for g-C_3N_4 and CdS are 4 and 1, respectively. The Eg of g-C_3N_4 and CdS photocatalysts can thus be obtained from the plots of $(ahv)^{1/2}$ and $(ahv)^2$ versus photon energy (hv), as shown in the inset of Fig. 3. The Eg of g-C_3N_4 and CdS are about 2.7 eV and 2.35 eV, respectively. The band positions of the photocatalysts can be calculated by the following empirical formulas $E_{CB} = X\text{-}0.5Eg\text{-}4.5$; $E_{VB} = X + 0.5Eg - 4.5$. From the calculation, it is known that the CB and VB of C_3N_4 are −1.13 eV and 1.57 eV, and the CB and VB of CdS are −0.49 eV and 1.86 eV, respectively.

3.1.3. SEM analysis

The morphology of the samples were investigated by SEM. Fig. 4 illustrates the respective SEM photographs of g-C_3N_4, CdS (10.0 wt.%)/g-C_3N_4 and CdS photocatalysts. From Fig. 4 (a), it is clear that the pure g-C_3N_4 displays aggregated morphologies, which are composed of block-based flakiness and particles. From Fig. 4 (b), it is clear that pure CdS sample shows significant aggregation with a diameter less than 0.5 μm. The morphology of CdS is similar to the spherical uniform particles. It is easy to see from Fig. 4(c) that the much smaller CdS nanoparticles spread uniformly on the surface of g-C_3N_4 samples and form the composite structures. Compared with the pure CdS particles, the CdS particles on the surface of g-C_3N_4 were smaller than those of pure CdS particles. It is proposed that g-C_3N_4 sample prevents the growth and development of CdS particles in the hydrothermal process. The EDS of CdS (10.0 wt.%)/g-C_3N_4 sample shown in Fig. 4 (d) demonstrates that the sample contains the signals of C, N, Cd and S elements.

3.1.4. TEM analysis

In order to investigate the interface of CdS (10.0 wt.%)/g-C_3N_4 sample, which showed the best photocatalytic activity, TEM and HRTEM characterization were performed. Fig. 5(a) gives an overview of the typical TEM image of the composite photocatalyst CdS/g-C_3N_4. It can be seen that the big block surface of g-C_3N_4 is covered by small particles of CdS, which is in accordance with the result of SEM image. The mean size of the CdS particles is approximately 50 nm. It is suggested that the charge transfer between the two semiconductors would be spatially smooth, leading to the improvement of photocatalytic activity. Fig. 5(b) shows HRTEM image of CdS (10.0 wt.%)/g-C_3N_4 sample. It is clear that the lattice plane with spacing of 0.325 nm matches the (0 0 2) crystallographic plane of hexagonal C_3N_4 (JCPDS card files no. 87-1526). The lattice fringes of 0.290 nm, 0.207 nm and 0.336 nm are attributed to the (2 0 0) plane of cubic CdS (JCPDS card files no. 10-0454), (1 1 0) and (0 0 2) planes of hexagonal CdS (JCPDS card files no. 41-1049), respectively. It is in accordance with the polycrystalline structure reflected by XRD patterns of CdS/g-C_3N_4 samples.

3.1.5. BET surface areas and pore size distributions

It can be seen from Fig. 6 that the nitrogen adsorption and desorption isotherms of the three samples are similar and all of them are type IV with hysteresis loops according to the IUPAC classification [56], indicating the presence of mesopores. All of the hysteresis loops can be categorized as type H3. It is known that the type H3 loop is observed with aggregates of plate like particles giving rise to slit-shaped pores. The BET specific surface area (S_{BET}) of the pristine g-C_3N_4 is about 4.0 $m^2\ g^{-1}$. After 10 wt.% CdS is coated, the S_{BET} of CdS (10.0 wt.%)/g-C_3N_4 increases to 7.1 $m^2\ g^{-1}$. The change in S_{BET} may be related to the small particle of CdS and different pore size distribution. As can be seen in the inset of Fig. 6, the pristine g-C_3N_4 contains mesopore range of 6–46 nm. The presence of small amount of CdS (10.0 wt%) can produce a lot of small mesopores (<6 nm).

3.2. Photocatalytic properties of CdS/g-C_3N_4 photocatalysts

The photocatalytic activity of the as-prepared photocatalyst is initially examined by the selective oxidation of benzyl alcohol to benzaldehyde and the reduction of nitrobenzene into aniline under

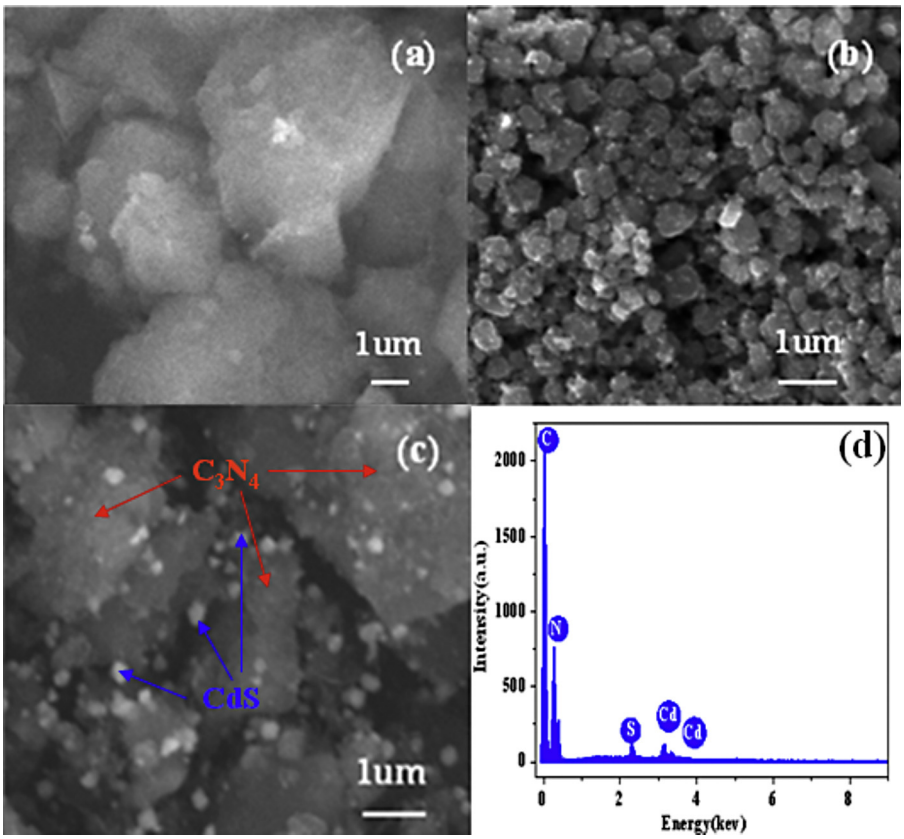

Fig. 4. SEM images of (a) g- C_3N_4, (b) CdS, (c) CdS (10.0 wt.%)/g-C_3N_4 samples and (d) EDS of CdS (10.0 wt.%)/g-C_3N_4 sample.

the irradiation of visible light ($\lambda > 420$ nm) for 4 h under N_2 purge condition. As shown in Fig. 7(A), pure g-C_3N_4, CdS and CdS/g-C_3N_4 samples all can realize the selective oxidation of benzyl alcohol to the corresponding benzaldehyde and the reduction of nitrobenzene into aniline. For the selective oxidation of benzyl alcohol to the benzaldehyde, it is clear that the conversion and yield increase with the increase in the amount of CdS from 1 to 10%. When the amount of CdS is higher than 10%, the conversion and yield decrease gradually. For pure g-C_3N_4, the conversion and yield are 9.3% and 7.7%, and for blank-CdS, the conversion and yield are 16.3% and 15.1%, respectively. Meanwhile, it also can be seen that the selectivity of pure CdS is higher than that of pure g-C_3N_4. When the amount of CdS is 1%, the conversion and yield of the sample is higher than those of the pure g-C_3N_4 and CdS. When the weight ratio of CdS is 10%, the conversion, yield and selectivity are higher than those of all the other photocatalysts. The conversion of benzyl alcohol and yield of benzaldehyde are about 48.0% and 44.6%, respectively. And the selectivity is higher than 90%.

For the reduction of nitrobenzene into aniline (Fig. 7(B)), the same trend as the selective oxidation of benzyl alcohol is occurred. Namely, the conversion and yield increase with the increase in the amount of CdS from 1 to 10%. When the amount of CdS is 10%, the conversion and yield are the highest. The conversion of nitrobenzene and yield of aniline are about 49.2% and 26.0%, respectively,

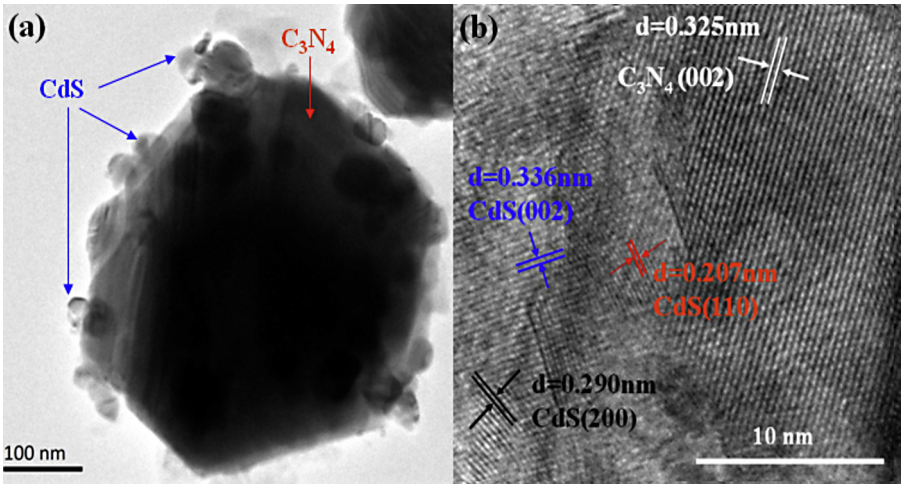

Fig. 5. TEM and HRTEM images of CdS (10.0 wt.%)/g-C_3N_4 sample.

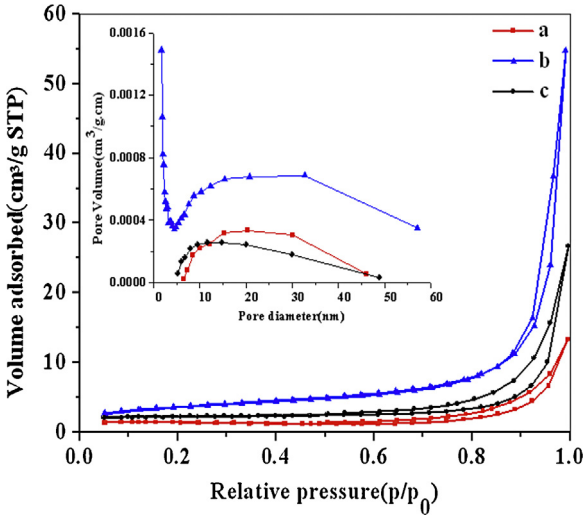

Fig. 6. Nitrogen adsorption–desorption isotherms and the corresponding pore size distribution curves (the inset) obtained from the desorption branches of the isotherms (a) C_3N_4, (b) CdS and (c) CdS (10.0 wt.%)/g-C_3N_4 samples.

which are higher than the values obtained from pure g-C_3N_4 (10.5% of conversion and 3.2% of yield) and blank-CdS (16.4% of conversion and 6.0% of yield). Further increase in the amount of CdS higher than 10.0 wt.% leads to a deterioration for the reduction of nitrobenzene into aniline.

When the amount of CdS in CdS/g-C_3N_4 samples is relatively high, the target product aldehyde may not be easily desorbed on the surface of photocatalysts due to the adsorption ability of sulfur species [57]. It is logical that the relatively high weight ratio of CdS in CdS/g-C_3N_4 samples would unavoidably reduce the contact surface of semiconductor g-C_3N_4 with the light illumination and lower the light intensity through the depth of reaction solution, which results in a decreased photocatalytic activity [58]. Considering the above two cases, further deep oxidation of aldehyde may occur, which leads to the decrease of selectivity, as reflected in the case of CdS (15.0 wt.%)/g-C_3N_4 and CdS (20.0 wt.%)/g-C_3N_4 samples. In accordance with the above results, the CdS (10.0 wt.%)/g-C_3N_4 photocatalysts is chosen to evaluate the photocatalytic activity for the selective oxidation of other benzylic and allylic alcohols.

Fig. 8 shows the photocatalytic performance of the selective oxidation of a range of alcohols (including benzylic alcohols and allylic alcohols) and the reduction of nitrobenzene into aniline over the CdS(10.0 wt.%)/g-C_3N_4 photocatalyst. It can be seen from Fig. 8(A) that the conversion and yield decrease as follows: p-methoxybenzyl alcohol > benzyl alcohol > p-chlorobenzyl alcohol > p-fluorobenzyl alcohol > cinnamyl alcohol. With the illumination for 4 h, the conversions of p-methoxybenzyl alcohol, benzyl alcohol, p-chlorobenzyl alcohol, p-fluorobenzyl alcohol and cinnamyl alcohol are 55.1, 48.0, 36.0, 32.0, 28.6, and the yields are 52.4, 44.6, 32.7, 23.0 and 14.5, respectively. However, the selectivity of p-methoxybenzyl alcohol, benzyl alcohol and p-chlorobenzyl alcohol are almost the same, and are higher than that of p-fluorobenzyl alcohol and cinnamyl alcohol. From Fig. 8, it is clear that the presence of a benzene ring seems to improve the selectivity. In general, the stronger the electronegativity, the easier the oxidation. It is known that the electronic effect of the functional group is as follows: $-OCH_3 > -H > -Cl > -F$. So the conversion, yield and selectivity of the reaction should be as follows: p-methoxybenzyl alcohol > benzyl alcohol > p-chlorobenzyl alcohol > p-fluorobenzyl alcohol. In the study, the results prove the above analysis. However, for allylic alcohol, such as cinnamyl alcohol, the selectivity is relatively low. This may result from $\pi-\pi$ conjugated effect, which is caused by the formation of benzene ring and C=C double bond, and then the $\pi-\pi$ conjugated effect influences the oxidation process of cinnamyl alcohol [21,22].

For the reduction of nitrobenzene, the conversion, yield and selectivity are the same as the trend of selective oxidation of a range of alcohols (Fig. 8 B). It seems that there should exist a certain relation between the selective oxidation and reduction. Namely, high conversion, yield and selectivity for the selective oxidation of alcohols should have high conversion, yield and selectivity for the reduction of nitrobenzene. For example, for the coupled system of p-methoxybenzyl alcohol and nitrobenzene, the conversion, yield and selectivity of reduction are 70.0, 40.0 and 57.1, respectively. They are higher than those of other coupled systems of alcohols and nitrobenzene. This may be attributed to the equilibrium relationship between selective oxidation and reduction due to dehydrogenation for the selective oxidation of alcohols and hydrogenation for the reduction of nitrobenzene.

In order to compare the photocatalytic performance between the samples prepared by hydrothermal and the samples prepared by mechanical mixing, the photocatalytic activity of CdS (1.0 wt.%)/g-C_3N_4, CdS (10 wt.%)/g-C_3N_4 and CdS (20 wt.%)/g-C_3N_4 photocatalysts prepared by ball milling method were investigated

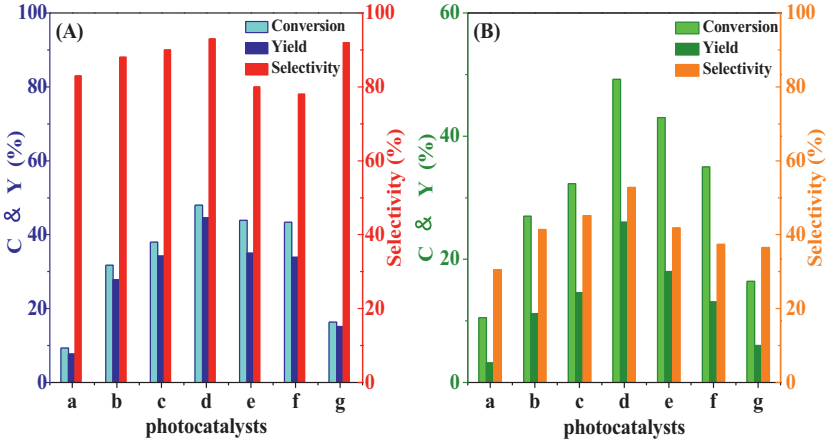

Fig. 7. Performance of the different samples for selective oxidation of benzyl alcohols to benzaldehyde and reduction of nitrobenzene into aniline under visible light irradiation ($\lambda > 420$ nm) for 4 h with N_2 purge condition. (A) benzyl alcohols, (B) nitrobenzene.
(a) g-C_3N_4, (b) CdS (1.0 wt.%)/g-C_3N_4, (c) CdS (5.0 wt.%)/g-C_3N_4, (d) CdS (10.0 wt.%)/g-C_3N_4, (e) CdS (15.0 wt.%)/g-C_3N_4, (f) CdS(20.0 wt.%)/g-C_3N_4, (g) CdS

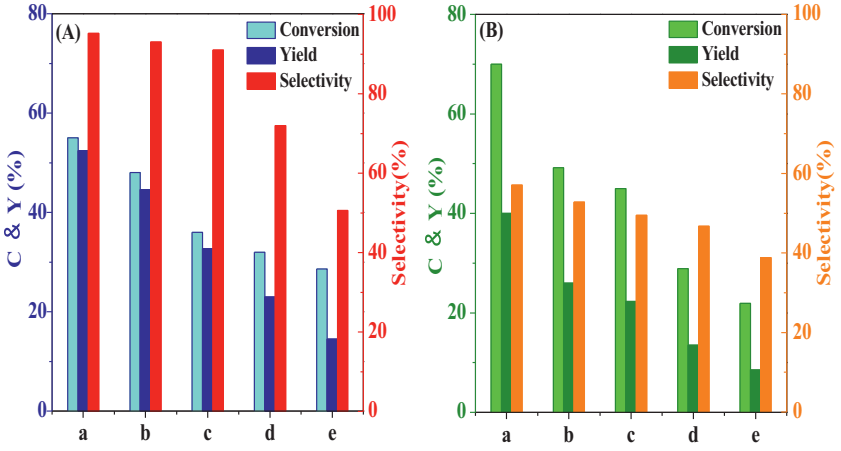

Fig. 8. Performance of CdS (10.0 wt.%)/g-C_3N_4 for selective oxidation of aromatic alcohols to aldehydes (A) and reduction of nitrobenzene into aniline (B) under visible light irradiation (λ > 420 nm) for 4 h with N_2 purge condition.
(a) p-methoxybenzyl alcohol; (b) benzyl alcohols; (c) p-chlorobenzyl alcohol;
(d) p-fluorobenzyl alcohol; (e) cinnamyl alcohol

[59,60]. The result showed that the photocatalytic performance of the samples is slightly lower than that of the samples prepared by hydrothermal method for selective oxidation of benzyl alcohol into benzaldehyde and reduction of nitrobenzene into aniline.

3.3. Stability of catalyst

The stability of CdS (10.0 wt.%)/g-C_3N_4 was investigated by XRD patterns of fresh and used samples and five successive cycles of experiments. As shown in Fig. 9, the XRD patterns of fresh and used 5 times samples have no obvious change. The cyclic experiments were carried out under the same conditions using CdS (10.0 wt.%)/g-C_3N_4 photocatalyst in order to determine the stability of the photocatalyst. After the reaction, the suspension was taken from the reaction kettle and centrifuged at 8000 rpm for 40 min to collect the catalyst. And then, the catalyst was washed with deionized water for three times. The results are shown in Fig. 10. It is clear that in the 5-cycle experiments, the conversion of benzyl alcohol and yield of benzaldehyde do not change obviously. Furthermore, no obvious decrease in the conversion and yield for the reduction of nitrobenzene into aniline were observed after the five-run test. Therefore, it can be concluded that the photocatalyst has good stability in the experimental conditions.

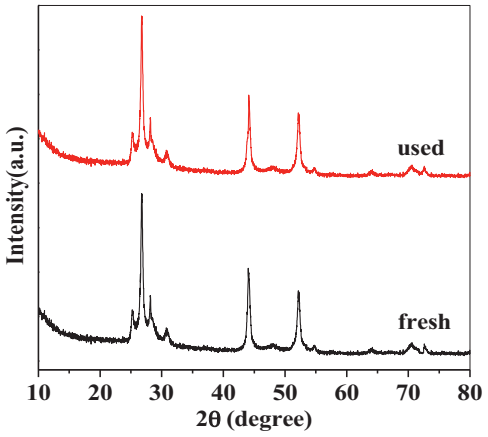

Fig. 9. XRD patterns of fresh and used 5 times samples.

3.4. Proposed reaction mechanism

A possible mechanism for the photocatalytic selective oxidation of alcohols and the reduction of nitrobenzene by CdS/g-C_3N_4 photocatalyst is illustrated in Fig. 11. Under the visible light illumination, both C_3N_4 and CdS can be excited and produce photogenerated

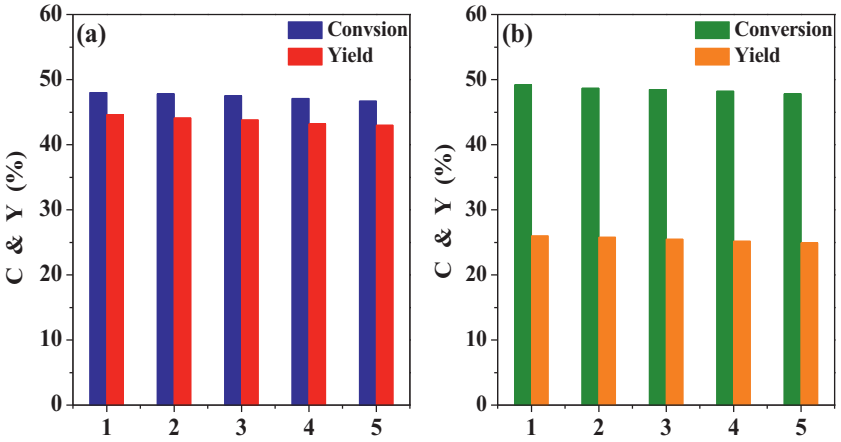

Fig. 10. Cyclic experiments of CdS (10.0 wt.%)/g-C_3N_4 sample for selective oxidation of benzyl alcohol to benzaldehyde and reduction of nitrobenzene into aniline.
(a) benzyl alcohol; (b) nitrobenzene

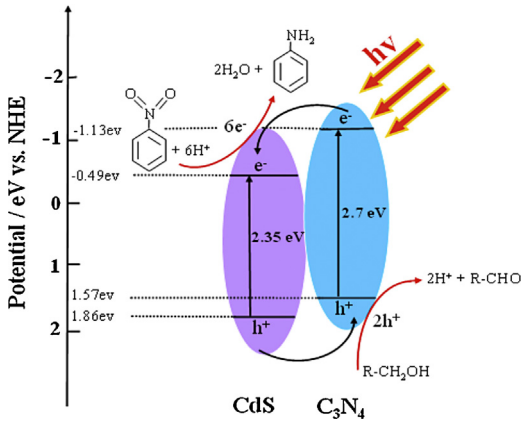

Fig. 11. Proposed mechanism of the selective oxidation alcohol and the reduction of nitrobenzene under N_2 purge condition.

electrons and holes. On account of the well-matched overlapping band structures and closely contacted interfaces, photoexcited electrons in the CB of C_3N_4 can directly transfer to the CB of CdS. Meanwhile, photoexcited holes in the VB of CdS spontaneously move to the VB of C_3N_4. In addition, the N_2 purge condition provides an anaerobic atmosphere for the reaction. Thus, the nitrobenzene has no opportunity to undergo the oxidation reaction. For the reduction of nitrobenzene, a photoinduced six-electron reduction process is involved [61]. Meanwhile, the photogenerated holes are quenched by the alcohols, which results in the aromatic alcohols removing hydrogen atoms, and then oxidized to the aldehyde [62]. At the same time, nitrobenzene obtains hydrogen atoms and loses the oxygen atoms, and consequently aniline is formed. In this process, the system will generate a small amount of H_2O. The whole process is shown in equations 8–11. It is clear that the photogenerated holes and photogenerated electrons should play the same crucial roles in the oxidation–reduction coupling process. Evidently, complete reduction of 1 mol nitrobenzene should require six mol electrons. Meanwhile, the same numbers of holes (six mols) are produced. According to the equation 11, it is known that the amount of aldehyde generated in this reaction system must be 3 times the amount of aniline. But in fact, due to the lag effect in this system, the generated amount of aldehyde and aniline are not strictly consistent with the above theoretical value.

$$2R{-}CH_2OH + 2\,h^+ \rightarrow R{-}CH_2O\bullet + R{-}CHOH\bullet + 2H^+ \quad (8)$$

$$R{-}CH_2O\bullet + R{-}CHOH\bullet + 2\,h^+ \rightarrow 2R{-}CHO + 2H^+ \quad (9)$$

In order to prove the effective separation of the photogenerated charges, the photoluminescence (PL) spectra of the samples were carried out [59,60]. The result is shown in Fig. 12. It is clear that the PL spectra of the samples have a strong emission peak at around 450 nm, which could be related to the recombination of the photoexcited electron–hole of g-C_3N_4. From Fig. 12, it can be seen that the PL intensity of CdS (10.0 wt.%)/g-C_3N_4 is lower than that of g-C_3N_4. It means that the recombination rate of the photoexcited electron-hole for CdS (10.0 wt.%)/g-C_3N_4 is lower than that of g-C_3N_4.

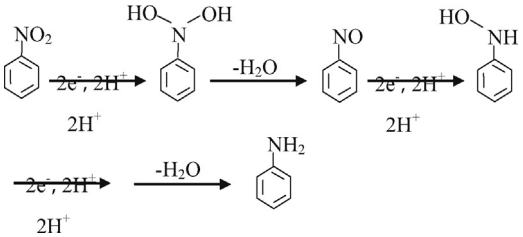

(10)

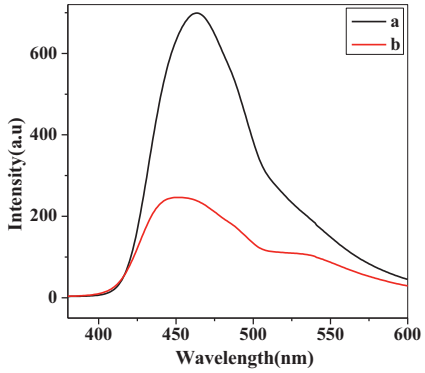

Fig. 12. Photoluminescence spectra of g-C_3N_4 (a) and CdS (10.0 wt.%)/g-C_3N_4 (b) samples.

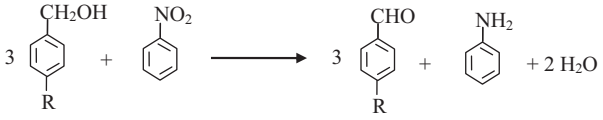

(11)

4. Conclusion

In summary, a coupled system for the selective oxidation of aromatic alcohols to aromatic aldehydes and the reduction of nitrobenzene into aniline was realized using CdS/g-C_3N_4 photocatalyst under visible light illumination. The selective oxidation of aromatic alcohol into aromatic aldehyde and the reduction of nitrobenzene into aniline are achieved by direct holes oxidation and direct electrons reduction, respectively. The CdS/g-C_3N_4 photocatalyst exhibits enhanced photocatalytic activity and excellent photostability under visible light illumination. This study has a guiding significance for the design of a coupled system which realizes selective oxidation and reduction of organics.

Acknowledgements

This study was supported by the National Natural Science Foundation of China (NSFC, grant No. 51172086, 21103060 and 51272081).

References

[1] A. Fujishima, K. Honda, Nature 238 (1972) 37–38.
[2] Y.J. Xu, Y.B. Zhuang, X.Z. Fu, J. Phys. Chem. C 114 (2010) 2669–2676.
[3] X.L. Fu, J.L. Long, X.X. Wang, D.Y.C. Leung, Z.X. Ding, L. Wu, Z.Z. Zhang, Z.H. Li, X.Z. Fu, Int. J. Hydrogen Energ. 22 (2008) 6484–6491.
[4] Y.B. Zhuang, H.Y. Song, G. Li, Y.J. Xu, Mater. Lett. 64 (2010) 2491–2493.
[5] Q.J. Xiang, J.G. Yu, M. Jaroniec, J. Am. Chem. Soc. 134 (2012) 6575–6578.
[6] Y.D. Hou, L. Wu, X.C. Wang, Z.X. Ding, Z.H. Li, X.Z. Fu, J. Catal. 250 (2007) 12–18.
[7] Q. Gu, X.L. Fu, X.X. Wang, S.F. Chen, Appl. Catal. B: Environ. 106 (2011) 689–696.
[8] S.G. Meng, D.Z. Li, X.Z. Zheng, J.X. Wang, J. Chen, J.L. Fang, Y. Shao, X.Z. Fu, J. Mater. Chem. A 1 (2013) 2744–2747.
[9] X.L. Fu, Y.F. Hu, Y.G. Yang, W. Liu, S.F. Chen, J. Hazard. Mater. 244–245 (2013) 102–110.
[10] X.W. Wang, G. Liu, Z.G. Chen, F. Li, L.Z. Wang, G.Q. Lu, H.M. Cheng, Chem. Commun. (2009) 3452–3454.
[11] S. Yurdakal, G. Palmisano, V. Loddo, V. Augugliaro, L. Palmisano, J. Am. Chem. Soc. 130 (2008) 1568–1569.
[12] A. Tanaka, K. Hashimoto, H. Kominami, J. Am. Chem. Soc. 134 (2012) 14526–14533.
[13] T. Kamegawa, H. Seto, S. Matsuura, H. Yamashita, Appl. Mater. Interfac. 4 (2012) 6635–6639.
[14] W.M. Wu, G.D. Liu, S.J. Liang, Y. Chen, L.J. Shen, H.R. Zheng, R.S. Yuan, Y.D. Hou, L. Wu, J. Catal. 290 (2012) 13–17.
[15] D.I. Enache, J.K. Edwards, P. Landon, B.S. Espriu, A.F. Carley, A.A. Herzing, M. Watanabe, C.J. Kiely, D.W. Knight, G.J. Hutchings, Science 311 (2012) 362–365.
[16] W.Y. Zhai, S.J. Xue, A.W. Zhu, Y.P. Luo, Y. Tian, ChemCatChem 3 (2011) 127–130.
[17] N. Zhang, S.Q. Liu, X.Z. Fu, Y.J. Xu, J. Phys. Chem. C 115 (2011) 22901–22909.

[18] M. Zhang, C.C. Chen, W.H. Ma, J.C. Zhao, Angew. Chem. Int. Ed. 120 (2008) 9876–9879.
[19] F.Z. Su, S.C. Mathew, G. Lipner, X.Z. Fu, M. Antonietti, S. Blechert, X.C. Wang, J. Am. Chem. Soc. 132 (2010) 16299–16301.
[20] P.F. Zhang, Y.T. Gong, H.R. Li, Z.R. Chen, Y. Wang, RSC Adv. 3 (2013) 5121–5126.
[21] N. Zhang, Y.H. Zhang, X.Y. Pan, X.Z. Fu, S.Q. Liu, Y.J. Xu, J. Phys. Chem. C 115 (2011) 23501–23511.
[22] N. Zhang, S.Q. Liu, X.Z. Fu, Y.J. Xu, J. Mater. Chem. 22 (2012) 5042–5052.
[23] Y.H. Zhang, N. Zhang, Z.R. Tang, Y.J. Xu, Chem. Sci. 3 (2012) 2812–2822.
[24] A.J. Hoffman, G. Mills, H. Yee, M.R. Hoffmann, J. Phys. Chem. 96 (1992) 5546–5552.
[25] M.H. Entezari, N. Ghows, Ultrason. Sonochem. 18 (2011) 127–134.
[26] W.T. Chen, T.T. Yang, Y.J. Hsu, Chem. Mater. 20 (2008) 7204–7206.
[27] T.T. Yang, W.T. Chen, Y.J. Hsu, K.H. Wei, T.Y. Lin, T.W. Lin, J. Phys. Chem. C 114 (2010) 11414–11420.
[28] L. Sheeney-Haj-Ichia, S. Pogorelova, Y. Gofer, I. Willner, Adv. Funct. Mater. 14 (2004) 416–424.
[29] P.V. Kamat, B. Shanghavi, J. Phys. Chem. B 101 (1997) 7675–7679.
[30] S.E. Habas, P.D. Yang, T. Mokari, J. Am. Chem. Soc. 130 (2008) 3294–3295.
[31] H.J. Yan, J.H. Yang, G.J. Ma, G.P. Wu, X. Zong, Z.B. Lei, J.Y. Shi, C. Li, J. Catal. 266 (2009) 165–168.
[32] D.R. Baker, P.V. Kamat, Adv. Funct. Mater. 19 (2009) 805–811.
[33] Y.L. Lee, Y.S. Lo, Adv. Funct. Mater. 19 (2009) 604–609.
[34] H. Tada, T. Mitsui, T. Kiyonaga, T. Akita, K. Tanaka, Nat. Mater. 5 (2006) 782–786.
[35] H. Kim, J. Kim, W. Kim, W. Choi, J. Phys. Chem. C 115 (2011) 9797–9805.
[36] J. Kobayashi, K. Kitaguchi, H. Tanaka, H. Tsuiki, A. Ueno, J. Chem. Soc. Faraday Trans. 83 (1987) 1395–1404.
[37] L. Jia, D.H. Wang, Y.X. Huang, A.W. Xu, H.Q. Yu, J. Phys. Chem. C 115 (2011) 11466–11473.
[38] L. Sheeney-Haj-Ichia, B. Basnar, I. Willner, Angew. Chem. Int. Ed. 44 (2005) 78–83.
[39] J.L. Wu, S. Bai, X.P. Shen, L. Jiang, Appl. Surf. Sci. 257 (2010) 747–751.
[40] A.N. Cao, Z. Liu, S.S. Chu, M.H. Wu, Z.M. Ye, Z.W. Cai, Y.L. Chang, S.F. Wang, Q.H. Gong, Y.F. Liu, Adv. Mater. 22 (2010) 103–106.
[41] E.A. Gelder, S.D. Jackson, C.M. Lok, Chem. Commun. (2005) 522–524.
[42] H.D. Burge, D.J. Collins, B.H. Davis, Ind. Eng. Chem. Prod. Res. Dev. 19 (1980) 389–391.
[43] S.G. Diao, W.Z. Qian, G.H. Luo, F. Wei, Y. Wang, Appl. Catal. A: Gen. 286 (2005) 30–35.
[44] J. Wisniak, M. Klein, Ind. Eng. Chem. Prod. Res. Dev. 23 (1984) 44–50.
[45] S. Balasubramanian, Luminescence behavior of tetraaza macrocylic nickel (II) complexes and non-linear Stern–Volmer quenching, J. Lumin. 106 (2004) 69–76.
[46] S. Füldner, P. Pohla, H. Bartling, S. Dankesreiter, R. Stadler, M. Gruber, A. Pfitzner, B. König, Green Chem. 13 (2011) 640–643.
[47] K. Imamura, T. Yoshikawa, K. Hashimoto, H. Kominami, Appl. Catal. B: Environ. 134–135 (2013) 193–197.
[48] L. Ge, C.C. Han, J. Liu, Appl. Catal. B: Environ. 108 (2011) 100–107.
[49] A. Sobczynski, A.J. Bard, A. Campion, M.A. Fox, T. Mallouk, S.E. Webber, J.M. White, J. Phys. Chem. 91 (1987) 3316–3320.
[50] J.Y. Zhang, Y.H. Wang, J. Jin, J. Zhang, Z. Lin, F. Huang, J.G. Yu, Appl. Mater. Interfac. 5 (2013) 10317–10324.
[51] J. Fu, B.B. Chang, Y.L. Tian, F.N. Xi, X.P. Dong, J. Mater. Chem. A 1 (2013) 3083–3090.
[52] S.W. Cao, Y.P. Yuan, J. Fang, M.M. Shahjamali, F.Y.C. Boey, J. Barber, S.C.J. Loo, C. Xue, Int. J. Hydrogen Energ. 38 (2013) 1258–1266.
[53] S.C. Yan, Z.S. Li, Z.G. Zou, Langmuir 26 (2010) 3894–3901.
[54] S.C. Yan, Z.S. Li, Z.G. Zou, Langmuir 25 (2009) 10397–10401.
[55] M.A. Butler, J. Appl. Phys. 48 (1977) 1914–1920.
[56] K.S.W. Sing, D.H. Everett, R.A.W. Haul, L. Moscou, R.A. Pierotti, J. Rouquerol, T. Siemieniewska, Pure Appl. Chem. 57 (1985) 603–619.
[57] T. Jin, T. Yamaguchi, K. Tanabe, J. Phys. Chem. 90 (1986) 4794–4796.
[58] L. Ge, J. Liu, Appl. Catal. B: Environ. 105 (2011) 289–297.
[59] S.F. Chen, Y.F. Hu, S.G. Meng, X.L. Fu, Appl. Catal. B: Environ. 150–151 (2014) 564–573.
[60] S.F. Chen, Y.G. Yang, W. Liu, J. Hazard. Mater. 186 (2011) 1560–1567.
[61] J.L. Ferry, W.H. Glaze, Langmuir 14 (1998) 3551–3555.
[62] H.W. Wei, H.C. Jiang, Z. Zheng, Q.Q. Zhao, Q.Y. Wu, J.H. Zhan, Mater. Res. Bull. 48 (2013) 1352–1356.